This article has been accepted for publication in a future issue of this journal, but has not been fully edited. Content may change prior to final publication. Citation information: DOI 10.1109/JLT.2017.2699619, Journal of Lightwave Technology

Highly sensitive fiber optic refractive index sensor using multicore coupled structures

D. A. May-Arrioja and J. R. Guzman-Sepulveda*

***Abstract* — In this paper we demonstrate highly sensitive refractive index (RI) sensing based on multicore coupled structures. Specifically, we use a seven-core fiber (SCF) as the sensing element. The interaction of the SCF and its surroundings is induced by controllably etching material from the cladding in order to expose its external cores. Thus, the sensor sensitivity can be tuned by simply controlling the etching depth. In our case, the cladding of a 10mm-long piece of SCF, spliced between two single-mode fibers (SMFs), was slowly removed until the remaining cladding around the external cores is only 2.5 µm. Sensitivity on the order of $1x10^4$ nm/RIU is experimentally demonstrated. These sensing architectures are compact, all-fiber, simple to fabricate, and highly sensitive. Based on our results RI changes of 10^{-4}-10^{-5} can be resolved with standard laboratory-graded equipment, which opens the possibility of using this type of sensing architectures in biological applications.**

***Index Terms* — Fiber optic sensor, Refractive index sensing, High sensitivity, Multicore coupled structures, Biological applications.**

I. INTRODUCTION

Refractive index (RI) sensing is of great importance in applications ranging from industrial quality control to chemical and biological analysis, biomedical applications, and specimen detection [1, 2]. Given its significance in a broad range of applications, RI sensing has been addressed by different means including optical fiber-based platforms which can be implemented in compact and sensitive architectures that are immune to the influence of external electromagnetic perturbations. The most prominent examples of fiber-based RI sensors traditionally used include sensing elements such as fiber Bragg gratings (FBG) and long-period fiber gratings (LPFG) [3, 4], in-fiber interferometers i.e. micro-machined cavities, and photonic crystal fibers (PCF) [5].

Grating-based RI sensors in general exhibit relatively low sensitivity for both LPFG and FBG when the grating is inscribed into standard SMFs [6]. This sensitivity can be significantly enhanced, for instance, by thinning the fiber grating in order to induce stronger interaction with the surroundings [7, 8], or by forcing a deeper coupling between the core and cladding modes by means of tilted gratings (340 nm/RIU) [9]. Nevertheless, the larger improvements have been reported for sensors where the grating is inscribed into PCFs [10]. For instance, sensitivity of 1,500-2,000 nm/RIU have been demonstrated with a simple LPFG-PCF where the liquid is infiltrated into the holes of the PCF without any particular optimization [11, 12]. The sensitivity of PCF-based sensors has also been mildly improved by using a PCF with concave core [13], and significantly enhanced up to 8,800 nm/RIU using four-wave mixing processes that do not require additional post-processing [14]. Interestingly, these sensors can be incorporated into lab-on-a-chip sensing platforms [15].

In terms of in-fiber interferometers, Fabry-Pérot and Mach-Zehnder architectures have been widely exploited for RI sensing since their fabrication can be done in a relatively simple way by tapering and micro-machining. Interestingly, despite interferometric approaches are typically associated to high-sensitivity sensing, this is not the case for PCF interferometers irrespective of whether they are operated in transmission (190.9 nm/RIU) [16], or reflection (6.67 nm/RIU) [17]. The sensitivity reported for RI sensors based on tapered SMFs is in general low as well (30 nm/RIU) [18-20], even if multiple tapers are cascaded (380 nm/RIU) [21, 22]. However, it has been proved that very large sensitivity can be achieved if the waist of millimeter-long tapers is reduced to only a few microns (>18,600 nm/RIU) [23]. In this arena of in-fiber interferometry, large sensitivity is typically achieved when using micro-machined cavities, where the manufacturing of the cavity can largely tune the sensor's sensitivity from values <2,000 nm/RIU [24, 25] to values >9,300 nm/RIU [26].

Regarding the use of structures with multiple cores, RI sensing based on a twin-core fiber has been reported [27]. This sensing architecture has a central core and a side core, which are not coupled, with the side core exposed to the external medium via chemical etching. By properly splicing this twin-core fiber to a SMF a Michelson interferometer is realized with a sensitivity of 826.8 nm/RIU. Sensors of similar nature i.e. two-core, where the external core is also selectively exposed to the surroundings, have been demonstrated with sensitivity >3,000 nm/RIU when the two single-mode cores are coupled i.e. in-fiber directional coupler [28].

Other RI sensing schemes with sensitivity comparable to the above-mentioned works have been demonstrated by using liquid-core structures [29, 30]. These techniques operate based on the changes observed in the propagating modes transmitted through the structure. These sensors exhibit high sensitivity

Manuscript received XXX XX, 2016; revised XXX XX, 2016. J.R.G.S. acknowledges the Mexican National Council of Science and Technology (CONACyT) for its partial support through a Ph.D. scholarship. The authors acknowledge the Microstructured Fibers and Devices Group at CREOL-UCF for kindly providing them with the optical fiber used in the experiments.

D. A. May-Arrioja is with Centro de Investigaciones en Optica, Aguascalientes, Ags. 20200, México; e-mail: darrioja@cio.mx

J. R. Guzman-Sepulveda is with CREOL, The College of Optics and Photonics, University of Central Florida. Orlando, Florida 32816, USA; e-mail: r.guzman@knights.ucf.edu

This article has been accepted for publication in a future issue of this journal, but has not been fully edited. Content may change prior to final publication. Citation information: DOI 10.1109/JLT.2017.2699619, Journal of Lightwave Technology

(>3,000 nm/RIU) at the expense of operating only over a limited range due to the RI of the liquids used to fill the capillaries has to be larger than the RI of the capillary tube. Overall, these architectures are suitable for high-index sensing, but cannot be used in most biological applications where aqueous solutions are commonly measured.

Interestingly, a dramatic increase in sensitivity has been recently predicted, by means of numerical simulations, for RI sensors using two-core PCF couplers as the sensing element [31-34]. These type of architectures effectively perform as a co-propagating directional coupler in which the so-called super modes of the structure interfere as they propagate. The numerical sensitivity ranges from 14,000 to 70,000 nm/RIU, and the highest experimentally demonstrated sensitivity is 30,000 nm/RIU [35]. Similar to the case of liquid-core structures, some of these PCF-coupler sensors, including the experimentally demonstrated one, are inherently limited by its principle of operation to be used only for liquids with RI higher than the waveguide material, i.e. 1.45, which prohibits using them in sensing of aqueous solutions with RI around 1.33 which are of biological relevance.

Other RI sensors having comparable sensitivity, but with the capability to operate in the RI range of water, have been demonstrated based on surface plasmon resonances (>50,000 nm/RIU; not fiber-based) [36]. Complementary to these plasmonic sensors, RI sensors operating based on lossy-mode resonances, using metallic oxides and polymer coatings on D-shaped fibers that enable exciting resonances with both polarizations and to generate multiple resonances within the spectral window of interest, have been reported with promising results [37-39]. These type of sensors have proved sensitivity >300,000 nm/RIU for RI around 1.44, and of 14,500 nm/RIU for RI around 1.33 [38].

In this paper we demonstrate highly sensitive RI sensing using a multicore coupled structure consisting of seven cores i.e. seven-core fiber (SCF). In general, sensors based on multicore coupled structures offer a number of advantages among which are their sinusoidal response, which is ideal for spectral interrogation, and their high sensitivity to small changes in the inter-coupling between the cores. Also, these sensing architectures are compact, all-fiber, simple to fabricate, and their sensitivity can be tuned by controllably etching the cladding of the multicore fiber section. The experimental results obtained in proof-of-concept experiments show that sensitivity on the order of $1\text{x}10^4$ nm/RIU can obtained, such that RI changes of 10^{-4}-10^{-5} can be resolved with standard laboratory-graded equipment. The sensitivity reported in the present work is lower than that in some of the above-described sensors. However, the fabrication of our sensor is simple and does not require additional enhancing mechanisms. More importantly, our sensor is not limited to operate in a particular RI range e.g. larger than the cladding, since the principle of operation relies on the modulation of the coupling coefficients of the inter-coupled single-mode waveguides from the exterior of the fiber. This opens the possibility of using this type of sensing architectures in biological applications.

II. Principle of Operation

The principle of operation of arbitrary dielectric coupled systems can be described within the frame of coupled mode theory. The linear interaction between the modes of N arbitrary, single-mode waveguides, as they propagate is described by the dynamic equation [40],

$$i\frac{d}{dz}\mathbf{A} = \overline{\mathbf{M}}\mathbf{A} \tag{1}$$

where **A** is a vector whose elements are the complex amplitudes of the electric field, at position z, for each core and **M** is the coupling matrix describing the interaction between pairs of cores. In its more general form, the coupling matrix **M** can be written as,

$$\overline{\mathbf{M}} = \begin{pmatrix} \beta_0 & \kappa_{01} & \kappa_{02} & \cdots & \kappa_{0(N-1)} \\ \kappa_{10} & \beta_1 & \kappa_{12} & \cdots & \kappa_{1(N-1)} \\ \kappa_{20} & \kappa_{21} & \beta_2 & \cdots & \kappa_{2(N-1)} \\ \vdots & \vdots & \vdots & \ddots & \vdots \\ \kappa_{(N-1)0} & \kappa_{(N-1)1} & \kappa_{(N-1)2} & \cdots & \beta_{(N-1)} \end{pmatrix} \tag{2}$$

where β_i is the propagation constant of the fundamental mode in the i-th waveguide and κ_{ij} is the coupling coefficient between the i-th and j-th cores. In the most general situation, the modes in the independent waveguides have different propagation constant i.e. $\beta_i \neq \beta_j$, and all of them interact with one another i.e. $\kappa_{ij} \neq 0$. Eq. (1) can be solved if all the elements of the coupling matrix and the initial complex amplitudes of the electric field are known. The matrix ***M*** entirely describes the interaction between the waveguides in a pair-wise manner and modeling an arbitrary coupled system can be reduced to the task of calculating the matrix elements.

The coupling coefficient between the i-th and j-th waveguides can be calculated rigorously through overlap integrals [41] or estimated in terms of the propagation constants of the even and odd coupled modes [42]. Alternatively, one can simplify the calculations for the specific geometry and characteristics of the coupled waveguides. According to the formulation of the mutual light-wave interactions between two parallel single-mode waveguides in the weakly guiding approximation, the coupling coefficient κ for two similar circular cores can be estimated as [43-46],

$$\kappa = \frac{\sqrt{2\Delta}}{a}\frac{U^2 K_0\left(sW/a\right)}{V^3\left[K_1\left(W\right)\right]^2} \tag{3}$$

where $\boldsymbol{a}$ is the radius of the cores, $\boldsymbol{s}$ is the center-to-center separation distance between them, and $\boldsymbol{\Delta}$ is the relative RI difference between core and cladding. $\boldsymbol{K_0}$ and $\boldsymbol{K_1}$ are the modified Hankel functions of order 0 and 1, respectively. The normalized frequency $\boldsymbol{V}$, and the normalized transverse propagation constants of the LP_{01} mode in the core and cladding, $\boldsymbol{U}$ and $\boldsymbol{W}$, respectively, are defined as [41, 46],

$$V = k_0 n_r a\sqrt{2\Delta} = \frac{2\pi}{\lambda_0}a\sqrt{n_r^2 - n_c^2} \tag{4a}$$

$$U \cong 2.405\exp\left[-\left(1-\frac{\sigma}{2}\right)\Big/V\right] \quad , \quad \sigma = 1-\left(\frac{n_c}{n_r}\right)^2 \tag{4b}$$

$$W = \left(V^2 - U^2\right)^{1/2} \tag{4c}$$

This article has been accepted for publication in a future issue of this journal, but has not been fully edited. Content may change prior to final publication. Citation information: DOI 10.1109/JLT.2017.2699619, Journal of Lightwave Technology

In general, the principle of operation of sensors based on coupled structures is implicit in the matrix elements (Eq. (2)) since both β_i and κ_{ij} depend at some extent on the environment in which the multicore structure sits. One can readily note that both optical and geometrical parameters determine the effective RI of the coupled modes and this, in turn, influences the coupling coefficient (Eq. (3)). These variations will result in changes of the overall response of the coupled system and can be used for sensing given the underlying dependence of the coupling coefficient on the external parameters. The approach outlined here conveniently provides means to assess spectrally operated devices, in which the response of coupled structures is evaluated within certain spectral window without the need of performing computationally expensive simulations. The conditions under which the expressions above can be safely used to produce reasonable estimates are typically met in real structures as it has been shown in a number different contexts besides sensing such as optoelectronic devices [44] and optical communication systems [47].

III. Simulations

Our simulation approach describes the experimental SCF in terms of circular cores with an effective diameter and effective separation distance between them such that the coupling coefficients are similar to those from the real fiber (which has hexagonal cores, as it will be shown later) which, strictly, would need to be calculated by means of more rigorous approaches. Rather than accurately modeling a particular real structure, our approach allows estimating the spectral sensitivity expected when the external cores are perturbed.

The solution to Eq. (1) can be simplified if the size of the cores is the same and the cores symmetrically disposed around a central core, as schematically shown in Fig. 1. Such structure can be described by two characteristic coupling coefficients, i.e. one for the coupling between external cores and another for the coupling between the central and external cores. In this scenario the N-by-N system of coupled differential equations obtained from Eq. (1) reduces to two equations that can be solved analytically for the amplitude of the electric field in the central core and (any of the) external cores [48],

$$a(z)=\exp(i\kappa z)\left[a_0\left(\cos(qz)-i\frac{C}{q}\sin(qz)\right)+b_0\left(i\frac{n\kappa}{q}\sin(qz)\right)\right] \quad (5a)$$

$$b(z)=\exp(iCz)\left[a_0\left(i\frac{\kappa}{q}\sin(qz)\right)+b_0\left(\cos(qz)+i\frac{C}{q}\sin(qz)\right)\right] \quad (5b)$$

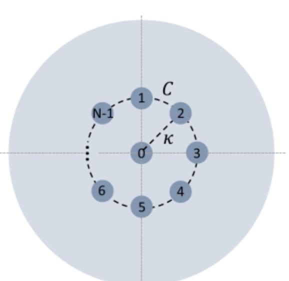

Fig 1. N-core coupled structure consisting of (N-1) cores symmetrically disposed around a central core. For similar cores, two coupling coefficients characterize the entire system –coupling between the central core and any of the external cores and coupling between adjacent external cores.

where $q=\sqrt{(C^2+n\kappa^2)}$ with n the number of cores around the central one, C and κ are the coupling coefficients for the external-external and external-central interaction, respectively, and a_0 and b_0 are the initial, i.e. at z = 0, amplitudes of the field in the central and the external cores. In order to resemble the experimental interrogation scheme, in which a section of multicore fiber (MCF) is spliced between two SMFs, only the central core is excited at z = 0 i.e. a_0 = 1 and b_0 = 0.

Fig. 2(a) shows the simulated spectral response of a 1 cm-long section of a SCF consisting of six cores symmetrically disposed around a central one. More specifically, the ‘spectral response’ refers to the normalized intensity transmitted through the central core of a section of SCF spliced between two SMFs within the spectral window from 14650 nm to 1665 nm. The RI of the cores and the cladding are taken as 1.45 and 1.444, respectively, and all the cores are assumed to be circular with an effective radius of 4.5 µm. The center-to-center separation distance between neighboring cores was set to an effective separation of 12 µm and kept constant throughout the simulation. The RI of all the cores as well as the RI of the cladding around the central core were kept constant. The simulations were performed by using Eqs. (3)-(5) and the only free parameter is an arbitrary, small variation of the effective RI ‘seen’ by the external cores. As a result of

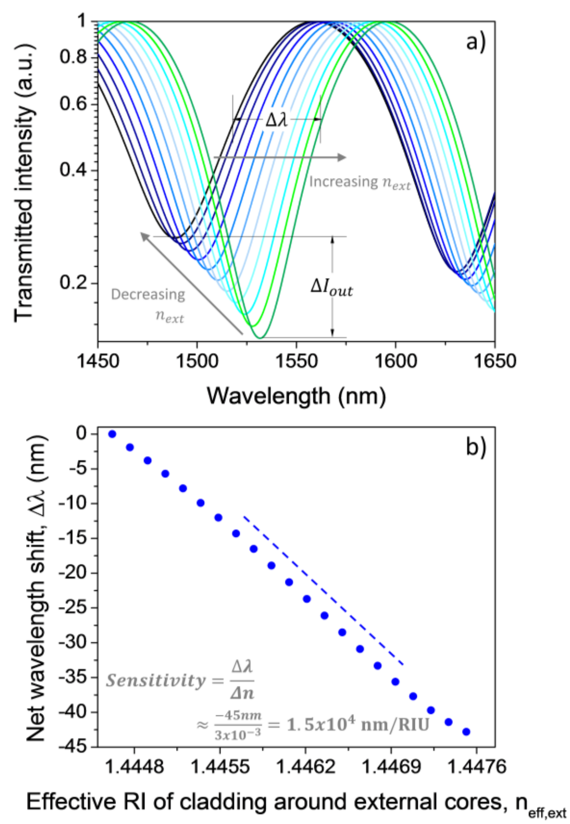

Fig. 2. Simulation of the spectral response of a 1 cm-long section of SCF, spliced between two SMFs and interrogated through its central core, for the case where the external cores experience an effective change in their RI. a) Spectral response – normalized intensity transmitted through the central core and b) net wavelength shift. The spectral response shows a red shift for increasing RI of the external medium. Conversely, the contrast decreases for decreasing RI of the surroundings due to a larger difference between the coupling constants C and κ and larger mismatch between the propagation constants of the central and external cores.

this small index variation both coupling constants, C and κ, change. Naturally, the coupling constant between adjacent external cores will be more affected.

This approach in which the external cores sense the environment and the central core is used for interrogation can be used to resemble the cases where i) a section of MCF surrounded by a medium of constant RI where the MCF cladding is progressively removed such that the interaction of the fiber with its environment progressively strengthens or ii) a section of MCF whose cladding has been etched down to a certain fixed diameter and the RI of the surrounding environment is modified. In both of these cases, larger variations in the effective RI of the external cores are induced as the thickness of the cladding decreases due to the stronger influence of the surroundings.

As shown in Fig. 2(a), the spectral response red-shifts for increasing external RI. Conversely, the contrast decreases for decreasing RI of the surroundings due to a larger difference between the coupling constants C and κ and larger mismatch between the propagation constants of the central and external cores. This is expected due to the fact that the central core remains practically unaltered. The simulations also suggests that an effective change in the RI of the cladding around the external cores of only $3x10^{-3}$ can produce a wavelength shift of several tens of nanometers, as shown in Fig. 2(b). This, in turn, allows us to estimate that sensitivities on the order of $-1.5x10^{4}$ nm/RIU can be achieved (slope of the straight line in Fig. 2(b)). Having this sensitivity translates into the capability to resolve RI changes of 10^{-4}–10^{-5} with standard optical spectrum analyzers (OSA) with resolution of 0.1 nm.

As mentioned before, we described the SCF structure in terms of circular cores with an effective diameter and effective separation distance between the cores that results in similar coupling coefficients to those from the real structure. Nevertheless, strictly speaking, a more rigorous approach in terms of overlap integrals of the electric field distribution would be necessary to calculate the coupling coefficient between cores of arbitrary shape [41]. In this regard, a number of different techniques can be implemented in order to estimate the field distribution and thus to be able to evaluate the overlap integrals involved in the rigorous calculation of the coupling coefficient [49-51]. Alternatively, one can evaluate the propagation of light through the structure directly by means of numerical approaches, e.g. finite element method.

IV. Experimental Results

The experimental setup employed for testing the performance of MCF-based spectrally operated RI sensors is schematically shown in Fig. 3(a). A fiber pigtailed super luminescent diode (SLD) is used to spectrally interrogate the MCF sensor. After the optical signal propagates through the MCF sensor, the transmitted spectrum (transmitted through its central core) is acquired using a standard OSA (Anritsu MS9740A) with a single-mode output fiber. This setup allows not only testing the sensors but also monitoring their response as the fiber cladding is being removed during etching.

The experiments were performed using a SCF provided by the Microstructured Fibers and Devices Group at CREOL-

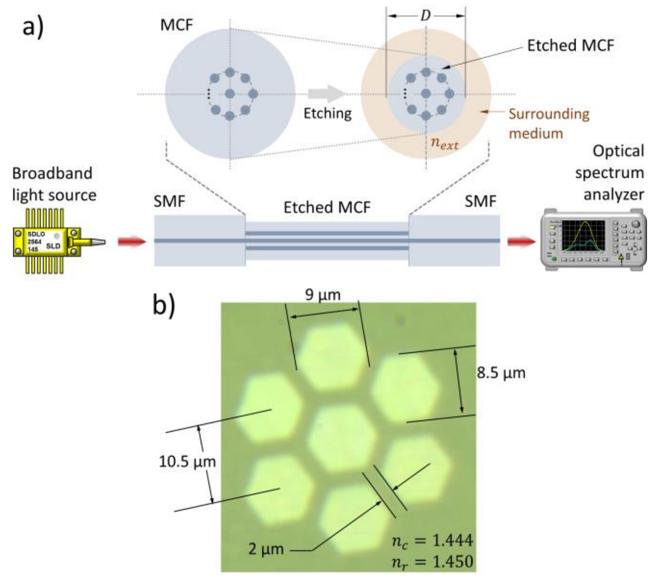

Fig. 3. a) Schematic of the experimental setup for spectrally operated RI multicore fiber sensors. The off-center cores of the MCF are exposed to interact with the surrounding by controllably etching material from the fiber cladding. The strength of the interaction can be controlled by means of this etching process – the sensitivity and contrast of the sensor response increase and decrease, respectively, with the etching depth. b) White-light microscope digital photo of the cross sections of the SCF used in the proof-of-concept experiments.

UCF. Fig. 3(b) shows a zoomed-in microscope digital photo of the cross-section of this fiber indicating the both the relevant dimensions and the RI of the core and cladding provided by the manufacturers at free-space wavelength of 1550 nm.

It is worth noting that the SCF used in the experiments has hexagonal cores (Fig. 3(b)), which is related to the fiber drawing process. However, given that the principle of operation of our sensor relies on the modulation of the inter-coupling between multiple single-mode dielectric waveguides, the shape of the cores is irrelevant. Cores with any arbitrary cross-sectional shape, as long as they are coupled, will meet the same sensing functionality. But, certainly, variations of the electric field distribution in the waveguides will lead to changes in the coupling coefficient due to the different overlap of the evanescent tails [42], which can alter the sensor's performance, e.g., sensitivity.

From the experimental standpoint MCFs with a central core have the advantage that they can be spliced directly to standard SMFs with negligible coupling losses, i.e., the position and numerical aperture of the cores closely match. This not only simplifies the fabrication and improves its reproducibility but also allows for a direct interrogation of the interaction between the MCF and its surroundings through the central core.

Proof-of-concept experiments were performed using the experimental setup from Fig. 3(a). The RI sensor was fabricated by first splicing a SMF to one end of the SCF. Then, using a micrometer controlled cleaver the other end of the SCF is cleaved to have a total length of 1 cm, and finally this end is spliced to another SMF. In the experiments RI sensing was done indirectly via thermo-optic effects based on the interaction of the etched multicore fiber with a surrounding medium having a well-defined thermo-optic coefficient (TOC). In this way, we can have a more accurate control on the experiments by using a surrounding medium with well calibrated RI and TOC.

The diameter of the SCF was reduced by etching the cladding using a commercial solution of buffered oxide etching (BOE) with average etching rate of 130 nm/min [28, 52]. The diameter of the SCF was reduced uniformly around its diameter, without any spatial selection for the etching, by covering the portion of exposed SMF and splices with commercial epoxy glue in order to expose only the SCF to etching. The amount of material removed was monitored by using an additional piece of SCF as control that was etched together with the sensor. The diameter of the control fiber was measured periodically under the microscope throughout the etching process. The etching was complete until we observed that the control fiber had a diameter of about 40 µm. At the end of the experiments the SCF sensor was cleaved using a focused ion beam (FIB) system, and the facet of the etched fiber was observed using a scanning electron microscope (SEM), as shown in Fig. 5(b).

The surrounding medium used in the experiments was Cargille index matching oil (Series AA, 1.452 at 653 nm and 25 °C, TOC -3.9x10-4 °C^{-1}). Fig. 4(a)-(b) shows the transmission spectra obtained in the experiments for etching times 360 min and 375 min, respectively. As shown in Fig. 4, the spectrum is blue shifted as the temperature is increased due to the negative TOC i.e. RI decreases with increasing temperature. Also, larger spectral shift is produced for the same RI change in the case of deeper etching due a stronger interaction with the surroundings.

Fig. 5(a) shows the net spectral shift obtained from the two etching times. It can be noticed that the sensitivity increases about four times, from -0.3 nm/°C to -1.25 nm/°C, approximately, when the etching time is increased from 360 min to 375 min. Fig. 5(b) shows a SEM picture of the cross section of the SCF after 375 min of etching. The diameter of the etched-fiber is about 41 µm, according to the scale bar from the SEM. The thickness of the cladding around the external cores is only 2.5 µm. It is worth highlighting that having tight control on the etching process is required to achieve this thickness since the etching rate dramatically increases close to the cores.

The temperature sensitivity calculated previously can be translated into RI units by simply taking the nominal TOC of the surrounding medium. For a TOC of $1\text{x}10^{-4}$ RIU/°C the sensitivities are estimated to be $3\text{x}10^{3}$ nm/RIU and $1.25\text{x}10^{4}$ nm/RIU for etching times 360 min to 375 min, respectively. A sensitivity of $1.25\text{x}10^{4}$ nm/RIU, which is among the highest values reported to date, is obtained when the cladding around the cores is only 2.5 µm. With this sensitivity it can be estimated that in principle RI changes on the order of 10^{-5} could be detected with a lab scale OSA with resolution of 0.1 nm. Since refractive index sensors capable to resolve changes on the order of 10^{-4}-10^{-5} or smaller can be used as label-free biosensors [10, 53-55], our approach presents a feasible option. In addition, given the short length of SCF used in our experiments (10 mm), the proposed sensor could be suitable for incorporation into lab-on-a-chip sensing platforms, as it has

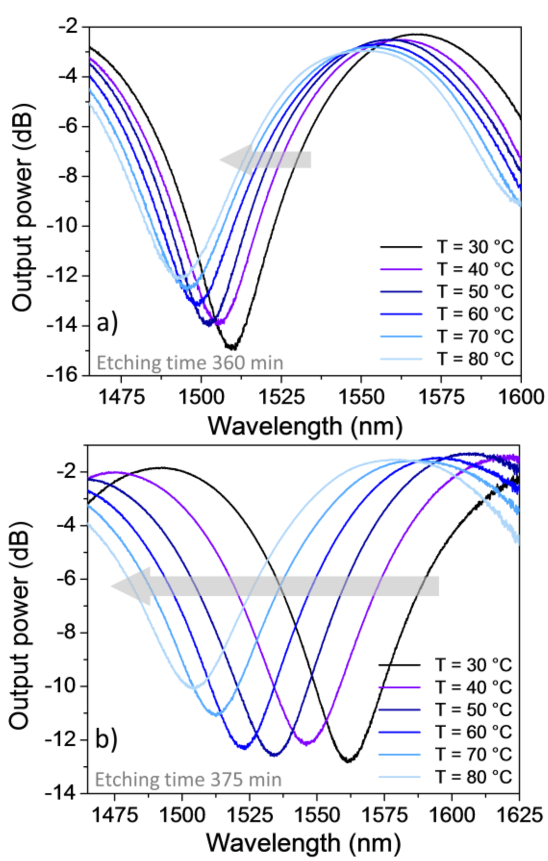

Fig. 4. Experimental spectral response of a section of SCF spliced between two SMFs for etching time a) 360 min and b) 375 min.

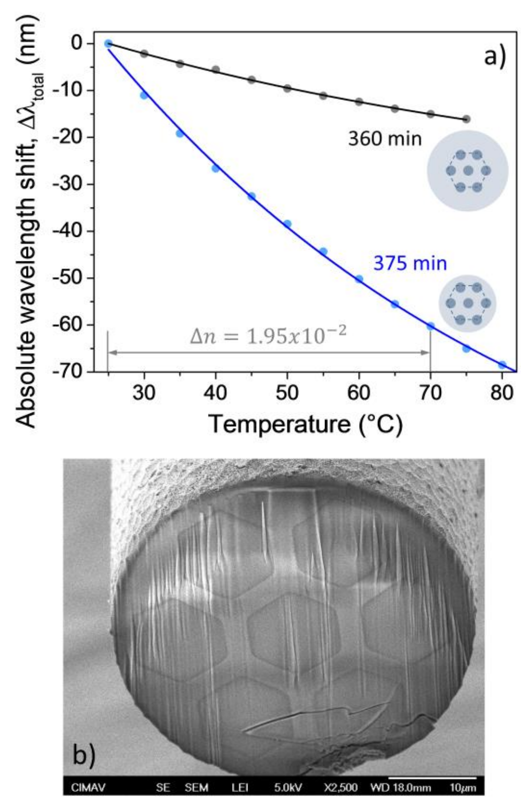

Fig. 5. a) Absolute wavelength shift of the SCF sensor for etching times 360 min and 375 min. b) SEM picture of the cross section of the SCF after 375 min of etching; the fiber diameter is 41 µm and the thickness of the cladding around the external cores is of only 2.5 µm. The interaction between the etched SCF and the surroundings is strong due to the thin cladding.

been demonstrated in previous studies using PCF-based sensors with longer lengths (16 mm) [15]. In both scenarios the surface of the SCF sensor would need to be functionalized in order to target a specific specimens.

Even though the sensitivity reported in our experiments can be considered sufficient for biological applications, we should emphasize that the sensitivity could be increased even further by inducing longer evanescent tails that result in a stronger interaction with the surrounding medium. This can be achieved, for instance, by depositing a thin layer of a high-index material around the etched fiber, as in lossy-mode resonant sensors [37-39] and other fiber sensors based on multimode interference effects [56-59]. Alternatively, one can deposit metal coatings as in the case of in-fiber plasmonic devices [60-63]. The use of properly designed coatings around the etched SCF could help to tune the operation and optimize the sensor's performance in the RI range of interest.

V. Conclusions

In summary, we demonstrated highly sensitive RI sensing based on multicore coupled structures. Specifically, in the experiments we used a seven-core fiber as the sensing element.

The principle of operation of these type of sensors was illustrated via a comprehensive approach based on coupled-mode theory that permits assessing the performance of spectrally operated fiber optic sensors without the need of performing computationally expensive simulations

In our approach material from the cladding of the multicore fiber is controllably removed in order to expose the external cores to interact with the external environment. The sensor sensitivity can be tuned by simply controlling the etching depth. Changes in the surrounding medium modulate the inter-coupling between the multiple cores and this, in turn, results in variations of the sensor's spectral response. In this way, the surrounding medium can be sensed through the external cores while the sensor is interrogated through the central one.

A maximum sensitivity of 1.25×10^4 nm/RIU was experimentally demonstrated. This sensitivity allows resolving RI changes of 10^{-4}-10^{-5} with standard laboratory-graded equipment. Given that our sensor is not limited to operate in a specific RI range, it can be used in biologically relevant applications. Finally, we would like to note that the sensitivity can be enhanced even further by employing special coatings that help to induce stronger interaction with the surroundings. Overall, our results are encouraging for further studies using other arrangements of the multicore coupled structures.

References

[1] S. Yin, C. Zhan, and P. B. Ruffin, "Fiber optic bio and chemical sensors," in *Fiber optic sensors*, S. S. Yin and P. Ruffin, Eds., Second ed Boca Raton, FL 33487-2742 US: CRC Press. Taylor & Francis Group., 2008, pp. 435-457.

[2] M. Ben-David and I. Gannot, "Optical Fibers for Biomedical Applications," in *Specialty optical fibers handbook*, A. Méndez and T. F. Morse, Eds., ed Burlington, MA 01803 US: Academic Press. Elsevier, 2011, pp. 699-734.

[3] L. Zhang, W. Zhang, and I. Bennion, "In-Fiber Grating Optic Sensors," in *Fiber optic sensors*, S. Yin, P. B. Ruffin, and T. S. Y. Francis, Eds., ed Boca Raton, FL 33487-2742 US: CRC Press. Taylor & Francis Group, 2008, pp. 109-162.

[4] Y.-J. Rao, "In-fibre Bragg grating sensors," *Measurement science and technology*, vol. 8, p. 355, 1997.

[5] S. Silva, P. Roriz, and O. Frazão, "Refractive index measurement of liquids based on microstructured optical fibers," in *Photonics*, 2014, pp. 516-529.

[6] X. Shu, L. Zhang, and I. Bennion, "Sensitivity characteristics of long-period fiber gratings," *Journal of Lightwave Technology*, vol. 20, pp. 255-266, 2002.

[7] K. S. Chiang, Y. Liu, M. N. Ng, and X. Dong, "Analysis of etched long-period fibre grating and its response to external refractive index," *Electronics Letters*, vol. 36, pp. 966-967, 2000.

[8] A. Iadicicco, A. Cusano, A. Cutolo, R. Bernini, and M. Giordano, "Thinned fiber Bragg gratings as high sensitivity refractive index sensor," *IEEE Photonics Technology Letters*, vol. 16, pp. 1149-1151, 2004.

[9] K. Zhou, L. Zhang, X. Chen, and I. Bennion, "Optic sensors of high refractive-index responsivity and low thermal cross sensitivity that use fiber Bragg gratings of> 80 tilted structures," *Optics letters*, vol. 31, pp. 1193-1195, 2006.

[10] L. Rindorf and O. Bang, "Sensitivity of photonic crystal fiber grating sensors: biosensing, refractive index, strain, and temperature sensing," *JOSA B*, vol. 25, pp. 310-324, 2008.

[11] Z. He, Y. Zhu, and H. Du, "Long-period gratings inscribed in air-and water-filled photonic crystal fiber for refractometric sensing of aqueous solution," *Applied Physics Letters*, vol. 92, p. 4105, 2008.

[12] L. Rindorf and O. Bang, "Highly sensitive refractometer with a photonic-crystal-fiber long-period grating," *Optics Letters*, vol. 33, pp. 563-565, 2008.

[13] J. Tian, Z. Lu, M. Quan, Y. Jiao, and Y. Yao, "Fast response Fabry–Perot interferometer microfluidic refractive index fiber sensor based on concave-core photonic crystal fiber," *Optics Express*, vol. 24, pp. 20132-20142, 2016.

[14] M. H. Frosz, A. Stefani, and O. Bang, "Highly sensitive and simple method for refractive index sensing of liquids in microstructured optical fibers using four-wave mixing," *Optics express*, vol. 19, pp. 10471-10484, 2011.

[15] L. Rindorf, P. E. Høiby, J. B. Jensen, L. H. Pedersen, O. Bang, and O. Geschke, "Towards biochips using microstructured optical fiber sensors," *Analytical and Bioanalytical Chemistry*, vol. 385, p. 1370, 2006.

[16] R. Jha, J. Villatoro, G. Badenes, and V. Pruneri, "Refractometry based on a photonic crystal fiber interferometer," *Optics Letters*, vol. 34, pp. 617-619, 2009.

[17] J. Villatoro, M. P. Kreuzer, R. Jha, V. P. Minkovich, V. Finazzi, G. Badenes, *et al.*, "Photonic crystal fiber interferometer for chemical vapor detection with high sensitivity," *Optics Express*, vol. 17, pp. 1447-1453, 2009.

[18] Z. Tian, S. S. Yam, and H.-P. Loock, "Refractive index sensor based on an abrupt taper Michelson interferometer in a single-mode fiber," *Optics letters*, vol. 33, pp. 1105-1107, 2008.

[19] P. Lu, L. Men, K. Sooley, and Q. Chen, "Tapered fiber Mach–Zehnder interferometer for simultaneous measurement of refractive index and temperature," *Applied Physics Letters*, vol. 94, p. 131110, 2009.

[20] Y. Li, L. Chen, E. Harris, and X. Bao, "Double-pass in-line fiber taper Mach–Zehnder interferometer sensor," *Photonics Technology Letters, IEEE,* vol. 22, pp. 1750-1752, 2010.

[21] D. Wu, T. Zhu, M. Deng, D.-W. Duan, L.-L. Shi, J. Yao*, et al.*, "Refractive index sensing based on Mach–Zehnder interferometer formed by three cascaded single-mode fiber tapers," *Applied optics,* vol. 50, pp. 1548-1553, 2011.

[22] V. Bhardwaj and V. K. Singh, "Fabrication and characterization of cascaded tapered Mach-Zehnder interferometer for refractive index sensing," *Sensors and Actuators A: Physical,* vol. 244, pp. 30-34, 2016.

[23] W. B. Ji, H. H. Liu, S. C. Tjin, K. K. Chow, and A. Lim, "Ultrahigh sensitivity refractive index sensor based on optical microfiber," *IEEE Photonics Technology Letters,* vol. 24, pp. 1872-1874, 2012.

[24] T. Wei, Y. Han, Y. Li, H.-L. Tsai, and H. Xiao, "Temperature-insensitive miniaturized fiber inline Fabry-Perot interferometer for highly sensitive refractive index measurement," *Optics Express,* vol. 16, pp. 5764-5769, 2008.

[25] W. Yuan, F. Wang, A. Savenko, D. H. Petersen, and O. Bang, "Note: Optical fiber milled by focused ion beam and its application for Fabry-Pérot refractive index sensor," *Review of Scientific Instruments,* vol. 82, p. 076103, 2011.

[26] Y. Wang, M. Yang, D. Wang, S. Liu, and P. Lu, "Fiber in-line Mach-Zehnder interferometer fabricated by femtosecond laser micromachining for refractive index measurement with high sensitivity," *JOSA B,* vol. 27, pp. 370-374, 2010.

[27] A. Zhou, Y. Zhang, G. Li, J. Yang, Y. Wang, F. Tian*, et al.*, "Optical refractometer based on an asymmetrical twin-core fiber Michelson interferometer," *Optics letters,* vol. 36, pp. 3221-3223, 2011.

[28] J. R. Guzmán-Sepúlveda, R. Guzmán-Cabrera, M. Torres-Cisneros, J. J. Sánchez-Mondragón, and D. A. May-Arrioja, "A Highly Sensitive Fiber Optic Sensor Based on Two-Core Fiber for Refractive Index Measurement," *Sensors,* vol. 13, pp. 14200-14213, 2013.

[29] H. Lee, M. Schmidt, P. Uebel, H. Tyagi, N. Joly, M. Scharrer*, et al.*, "Optofluidic refractive-index sensor in step-index fiber with parallel hollow micro-channel," *Optics express,* vol. 19, pp. 8200-8207, 2011.

[30] M. A. Fuentes-Fuentes, D. A. May-Arrioja, J. R. Guzman-Sepulveda, M. Torres-Cisneros, and J. J. Sánchez-Mondragón, "Highly Sensitive Liquid Core Temperature Sensor Based on Multimode Interference Effects," *Sensors,* vol. 15, pp. 26929-26939, 2015.

[31] W. Yuan, G. E. Town, and O. Bang, "Refractive index sensing in an all-solid twin-core photonic bandgap fiber," *IEEE Sensors Journal,* vol. 10, pp. 1192-1199, 2010.

[32] G. E. Town, W. Yuan, R. McCosker, and O. Bang, "Microstructured optical fiber refractive index sensor," *Optics letters,* vol. 35, pp. 856-858, 2010.

[33] H. Wang, X. Yan, S. Li, G. An, and X. Zhang, "High Sensitivity Refractive Index Sensor Based on Dual-Core Photonic Crystal Fiber with Hexagonal Lattice," *Sensors,* vol. 16, p. 1655, 2016.

[34] G. An, S. Li, X. Yan, X. Zhang, Z. Yuan, and Y. Zhang, "High-sensitivity and tunable refractive index sensor based on dual-core photonic crystal fiber," *JOSA B,* vol. 33, pp. 1330-1334, 2016.

[35] D. K. Wu, B. T. Kuhlmey, and B. J. Eggleton, "Ultrasensitive photonic crystal fiber refractive index sensor," *Optics letters,* vol. 34, pp. 322-324, 2009.

[36] R. Slavík and J. Homola, "Ultrahigh resolution long range surface plasmon-based sensor," *Sensors and Actuators B: Chemical*, vol. 123, pp. 10-12, 2007.

[37] P. Zubiate, C. Zamarreño, I. Del Villar, I. Matias, and F. Arregui, "High sensitive refractometers based on lossy mode resonances (LMRs) supported by ITO coated D-shaped optical fibers," *Optics express*, vol. 23, pp. 8045-8050, 2015.

[38] F. J. Arregui, I. Del Villar, C. R. Zamarreño, P. Zubiate, and I. R. Matias, "Giant sensitivity of optical fiber sensors by means of lossy mode resonance," *Sensors and Actuators B: Chemical*, vol. 232, pp. 660-665, 2016.

[39] I. Del Villar, F. J. Arregui, C. R. Zamarreño, J. M. Corres, C. Bariain, J. Goicoechea, *et al.*, "Optical sensors based on lossy-mode resonances," *Sensors and Actuators B: Chemical*, vol. 240, pp. 174-185, 2017.

[40] N. Kishi and E. Yamashita, "A simple coupled-mode analysis method for multiple-core optical fiber and coupled dielectric waveguide structures," in *Microwave Symposium Digest, 1988., IEEE MTT-S International*, 1988, pp. 739-742.

[41] K. Okamoto, "Coupled Mode Theory," in *Fundamentals of optical waveguides*, Second ed Burlington, MA 01803, USA: Academic Press. Elsevier, 2006, pp. 159-208.

[42] A. Hardy and W. Streifer, "Coupled mode theory of parallel waveguides," *Lightwave Technology, Journal of,* vol. 3, pp. 1135-1146, 1985.

[43] A. W. Snyder, "Coupled-mode theory for optical fibers," *JOSA*, vol. 62, pp. 1267-1277, 1972.

[44] H. Kogelnik and R. V. Schmidt, "Switched directional couplers with alternating Δβ," *Quantum Electronics, IEEE Journal of,* vol. 12, pp. 396-401, 1976.

[45] A. Snyder and P. Richmond, "Effect of anomalous dispersion on visual photoreceptors," *JOSA,* vol. 62, pp. 1278-1283, 1972.

[46] Y. Murakami and S. Sudo, "Coupling characteristics measurements between curved waveguides using a two-core fiber coupler," *Applied optics,* vol. 20, pp. 417-422, 1981.

[47] C. Xia, N. Bai, I. Ozdur, X. Zhou, and G. Li, "Supermodes for optical transmission," *Optics express,* vol. 19, pp. 16653-16664, 2011.

[48] A. Perez-Leija, J. Hernandez-Herrejon, H. Moya-Cessa, A. Szameit, and D. N. Christodoulides, "Generating photon-encoded W states in multiport waveguide-array systems," *Physical Review A,* vol. 87, p. 013842, 2013.

[49] L. Eyges, P. Gianino, and P. Wintersteiner, "Modes of dielectric waveguides of arbitrary cross sectional shape," *JOSA,* vol. 69, pp. 1226-1235, 1979.

[50] S. M. Saad, "Review of numerical methods for the analysis of arbitrarily-shaped microwave and optical dielectric waveguides," *IEEE transactions on microwave theory and techniques,* vol. 33, pp. 894-899, 1985.

[51] C. H. Henry and B. H. Verbeek, "Solution of the scalar wave equation for arbitrarily shaped dielectric waveguides by two-dimensional Fourier analysis," *Journal of Lightwave Technology,* vol. 7, pp. 308-313, 1989.

[52] K. R. Williams, K. Gupta, and M. Wasilik, "Etch rates for micromachining processing-Part II," *Journal of microelectromechanical systems,* vol. 12, pp. 761-778, 2003.

This article has been accepted for publication in a future issue of this journal, but has not been fully edited. Content may change prior to final publication. Citation information: DOI 10.1109/JLT.2017.2699619, Journal of Lightwave Technology

[53] L. Rindorf, J. B. Jensen, M. Dufva, L. H. Pedersen, P. E. Høiby, and O. Bang, "Photonic crystal fiber long-period gratings for biochemical sensing," *Optics Express,* vol. 14, pp. 8224-8231, 2006.

[54] J. R. Ott, M. Heuck, C. Agger, P. D. Rasmussen, and O. Bang, "Label-free and selective nonlinear fiber-optical biosensing," *Optics express,* vol. 16, pp. 20834-20847, 2008.

[55] C. Markos, W. Yuan, K. Vlachos, G. E. Town, and O. Bang, "Label-free biosensing with high sensitivity in dual-core microstructured polymer optical fibers," *Optics express,* vol. 19, pp. 7790-7798, 2011.

[56] I. Del Villar, A. B. Socorro, J. Corres, F. Arregui, and I. Matias, "Optimization of sensors based on multimode interference in single-mode–multimode–single-mode structure," *Lightwave Technology, Journal of,* vol. 31, pp. 3460-3468, 2013.

[57] I. Del Villar, A. B. Socorro, J. M. Corres, F. J. Arregui, and I. R. Matias, "Refractometric sensors based on multimode interference in a thin-film coated single-mode–multimode–single-mode structure with reflection configuration," *Applied optics*, vol. 53, pp. 3913-3919, 2014.

[58] A. J. R. Rodríguez, O. Baldovino-Pantaleón, R. F. D. Cruz, C. R. Zamarreño, I. R. Matías, and D. A. May-Arrioja, "Gasohol quality control for real time applications by means of a multimode interference fiber sensor," *Sensors,* vol. 14, pp. 17817-17828, 2014.

[59] A. Socorro, I. Del Villar, J. Corres, F. Arregui, and I. Matias, "Sensitivity enhancement in a multimode interference-based SMS fibre structure coated with a thin-film: theoretical and experimental study," *Sensors and Actuators B: Chemical,* vol. 190, pp. 363-369, 2014.

[60] A. K. Sharma, R. Jha, and B. Gupta, "Fiber-optic sensors based on surface plasmon resonance: a comprehensive review," *Sensors Journal, IEEE,* vol. 7, pp. 1118-1129, 2007.

[61] X. Yu, Y. Zhang, S. Pan, P. Shum, M. Yan, Y. Leviatan, *et al.*, "A selectively coated photonic crystal fiber based surface plasmon resonance sensor," *Journal of Optics,* vol. 12, p. 015005, 2009.

[62] A. Dıez, M. Andres, and J. Cruz, "In-line fiber-optic sensors based on the excitation of surface plasma modes in metal-coated tapered fibers," *Sensors and Actuators B: Chemical*, vol. 73, pp. 95-99, 2001.

[63] D. Monzón-Hernández, J. Villatoro, D. Talavera, and D. Luna-Moreno, "Optical-fiber surface-plasmon resonance sensor with multiple resonance peaks," *Applied optics*, vol. 43, pp. 1216-1220, 2004.